Chapter 2
Wave Propagation in Anisotropic Media

Abstract Modern turbine blades are manufactured from single-crystal nickel-based superalloys for the excellent mechanical properties these materials exhibit at elevated temperatures. However, single-crystal materials are highly elastically anisotropic, meaning the elastic proprieties vary with direction. Wave propagation in anisotropic materials is significantly more complex than in isotropic materials. This severely complicates the inspection of these materials using ultrasound NDE methods. To enable the reliable inspection of single-crystal turbine blades with ultrasound, the propagation of ultrasonic waves in anisotropic material must be fully understood. In this chapter, the theory of bulk wave propagation in both isotropic and anisotropic solid materials is presented. Initially, a brief background of the research in wave propagation in solids is laid out to provide a historical context for this thesis. A short theory of bulk wave propagation is given and the important concepts of group and phase velocities are explained. Analytical models are then developed to describe wave propagation in anisotropic materials. Specifically, the developed analytical models simulate the variation in velocity with direction and the variation in beam amplitude from a point-force acting on the surface of an anisotropic material. These models are utilised in subsequent chapters to correct ultrasonic array imaging algorithms for the inspection of anisotropic materials. Finally, the analytical models are validated against numerical finite-element models.

2.1 Introduction

The history of research on wave propagation in anisotropic materials is linked with the development of the theory of elasticity in the early nineteenth century [1]. Early work by Green in 1839 showed that three wave modes could exist in a general anisotropic medium [2]. In 1877, Christoffel described the variation in the

C. Lane, *The Development of a 2D Ultrasonic Array Inspection for Single Crystal Turbine Blades*, Springer Theses, DOI: 10.1007/978-3-319-02517-9_2,

velocity of wavefronts in anisotropic media with the wavefront normal direction [3]. He developed mathematical formulae to compute this velocity, referred to as the phase velocity, using plane wave analysis.

The subsequent work on the theory of wave propagation in solids after this period was primarily concerned with and influenced by the fields of seismology and geophysics, with specific discoveries by scientists such as Rayleigh, Lamb and Love [4]. It has been suggested that as the elastic anisotropy of the Earth's crust is relatively small, little work was conducted on wave propagation in anisotropic solids during 1880–1910 [5]. Lord Kelvin began to investigate wave propagation in anisotropic media and reproduced Christoffel's findings in his Baltimore lectures in 1904 but concluded: 'the dynamics of elastic waves is a fine subject for investigation and I am sorry to pass from it now'[6].[1]

Very little progress was made until the 1950s when interest was revived due to the development of piezoelectric transducers and ultrasonic NDE methods. The ultrasonic inspection of anisotropic materials showed discrepancies between the theoretical knowledge and experimental findings. In the mid 1950s Musgrave [7] and Synge [8] used a wave energy based approach to compute the velocity of energy propagation in anisotropic solids which could then be shown to be equal to the group velocity in non-dispersive waves. In the 1960s, Merkulov developed a simplified derivation to compute the equation for the group velocity [9]. Merkulov also investigated the reflections of waves at the interfaces of an anisotropic solid and this was reviewed in more detail in 1968 by Fedorov [10].

In 1959, Buchwald was the first researcher to perform a detailed investigation of waves propagating from a point-force in an anisotropic elastic solid [11]. Using an asymptotic method developed by Lighthill [12], Buchwald derived an expression for the far-field amplitude of a wave excited by a point-force inside an infinite anisotropic solid. In 1971, Burridge used the Cagniard de-Hoop method to compute the amplitude of waves propagating from a point-force acting on the surface of an anisotropic half-space [13, 14]. Wu et al. developed a simplified approach to compute the far-field radiation for the same situation based on the reflection coefficients of waves at an interface of an anisotropic medium and the reciprocity theorem [15, 16].

The fundamental theory of wave propagation in anisotropic media thus is well understood and documented. For thorough discussions see [5, 17, 18]. Much of the current research in ultrasonic inspection of anisotropic components applies this theory to real applications and inspections. This will be discussed in the next chapter. What will be presented here is the theory of wave propagation that is required for this project, namely, the anisotropic velocity variation in bulk waves and the amplitude of bulk waves propagating from a point-force on an infinite anisotropic half-space. The analytical models are developed for both of these situations and are applied to CMSX-4 which is a single crystal nickel-based

[1] It may be of interest to note that Lord Kelvin did not approve of the prefix *an* for describing a non-isotropic solid. 'If we used this in English we should have to say: "An anisotropic solid is not an isotropic solid."' Instead Kelvin preferred the use of aeolotropic from the Greek αιόλος meaning variegated or different and τρόποζ meaning direction.

superalloy. The analytical models will be validated by comparing them to finite element models. The theory of surface waves or guided waves in anisotropic solids are not considered as they are not relevant to this thesis but references [17, 19] discuss these topics.

2.2 Bulk Waves in Anisotropic Solids

2.2.1 Bulk Wave Propagation in Isotropic and Anisotropic Solids

All metallic crystals are inherently anisotropic due to the directional differences in inter-atomic stiffness in the crystal structure. However, in conventionally cast engineering metals the microstructure is formed from many randomly orientated crystals, otherwise referred to as *grains*. In these polycrystalline materials, where the orientation of individual crystals is random, the mechanical properties on the macroscopic scale are independent of direction. Therefore, these materials are isotropic. In the case of ultrasonic wave propagation, when the ultrasonic wavelength is much greater than the grain size, isotropic assumptions are quite valid. Other metallic components, like single crystals or polycrystalline components, where the crystals in the microstructure material have a dominant orientation (for example directionally solidified castings, rolled materials or austenitic steel welds), exhibit highly anisotropic properties.

Bulk waves propagate in isotropic materials with equal velocity in every direction. Wave energy may propagate in two modes: longitudinal and shear. The faster mode is the longitudinal mode where the vibration of particles is *parallel* to the propagation of wave energy. The shear mode is the slower mode where the particle vibrations are *normal* to propagation direction. The direction of the particle vibration is referred to as the polarization.

The velocities, c_l and c_s, of the two bulk wave modes, where the sub-scripts l and s indicate longitudinal and shear modes respectively, can be computed using two elastic properties of the material, for example Young's Modulus E and Poisson's ratio υ, and the material density ρ using [20]:

$$c_l = \left(\frac{E(1-v)}{\rho(1+v)(1-2v)} \right)^{\frac{1}{2}} \tag{2.1}$$

$$c_s = \left(\frac{E}{2\rho(1+v)} \right)^{\frac{1}{2}} \tag{2.2}$$

The wave propagation in anisotropic media is substantially different to the isotropic case. The most significant difference is that elastic waves propagate with a velocity that depends on direction. Furthermore, unlike the isotropic case, three wave modes can propagate: one longitudinal and two shear waves. However, these

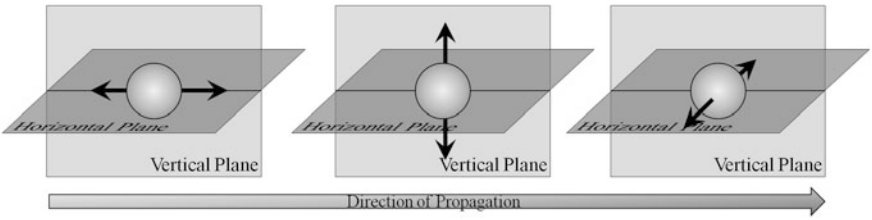

Fig. 2.1 Schematic diagram showing (from *left to right*) pure bulk wave propagation modes with longitudinal, shear-vertical and shear-horizontal polarization

modes are not necessarily pure modes as the particle vibration, or *polarization*, is neither parallel nor perpendicular to the propagation direction. In practice the anisotropic modes do show similarities to the isotropic modes and in these cases are referred to as quasi-longitudinal and quasi-shear. The quasi-shear modes are often distinguished further by whether they are primarily horizontally or vertically polarized. The polarization convention used for pure-modes is shown schematically in Fig. 2.1. The wavefronts of these quasi-modes generally do not lie normal to the energy propagating direction and hence the phase and group velocities do not coincide. These terms are explained in the next section. The phase and group velocities of waves in anisotropic solids can be computed from the material density and the elastic tensor that relates elastic stress and strain. In general there are up to 21 independent elastic constants in an anisotropic solid. However, most common engineering materials exhibit a lower degree of anisotropy and can therefore be described by fewer independent constants as shown in Table 2.1.

2.2.2 Phase and Group Velocity

The phase and group velocities are generally different in an anisotropic material and therefore a clear distinction between the two must be made to ensure the correct velocity profile is used when imaging with an ultrasonic array.

As a wave propagates in an elastic solid, particles within the material undergo a cyclic displacement. Particles at the same point within the cycle are said to have equal phase. Lines connecting particle of equal phase are referred as wavefronts. The velocity of the wavefront in the direction normal to the wavefront is known as the phase velocity. The spatial frequency of the wavefronts is referred to as the wavenumber. The wavenumber k of a wave propagating with phase velocity c and angular frequency ω is given by:

$$k = \frac{\omega}{c} \tag{2.3}$$

The group velocity is the velocity at which the envelope of a wave packet propagates. Figure 2.2 illustrates what is meant by the envelope of the wave packet.

Table 2.1 Anisotropic Materials

Material	Number of independent elastic constants	Engineering examples
Triclinic	21	–
Monoclinic	13	–
Orthotropic	9	–
Triagonal	7	–
Tetragonal	6	Yttria-stabilized zirconia for thermal barrier coatings
Transversely isotropic	5	Centrifugally cast stainless steel, welds
Hexagonal	5	Directional solidified castings
Cubic	3	Single crystal nickel castings
Isotropic	2	Polycrystalline metals

Auld [17] explains the concept of phase and group velocity mathematically by considering a modulated wave constructed of two waves of slightly different values of k and ω:

$$cos(kx - \omega t) + cos((k + \delta k)x - (\omega + \delta\omega)t) \tag{2.4}$$

Using the cosine rule, the equation describing the modulated wave is given by:

$$cos\left\{\left(k + \frac{\delta k}{2}\right)x - \left(\omega + \frac{\delta\omega}{2}\right)t\right\} cos\left\{\left(\frac{\delta k}{2}\right)x - \left(\frac{\delta\omega}{2}\right)t\right\} \tag{2.5}$$

The first cosine term in this equation is the high frequency carrier wave and the second term is the lower frequency modulation envelope. The velocity of the high frequency carrier wave can be seen to tend to the phase velocity as the small differences in ω and k tend to zero:

$$\frac{\omega + \frac{\delta\omega}{2}}{k + \frac{\delta k}{2}} \rightarrow \frac{\omega}{k} = c \tag{2.6}$$

The group velocity is the velocity of the lower frequency modulation envelope which, as the differences again tend to zero, is given by:

$$V = \frac{\delta\omega}{\delta k} \rightarrow \frac{\partial\omega}{\partial k} \tag{2.7}$$

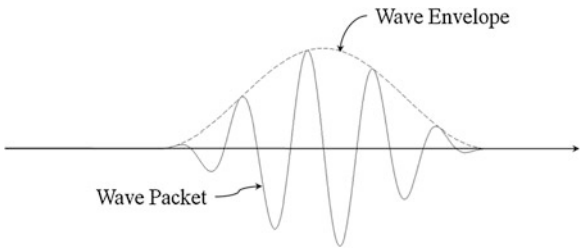

Fig. 2.2 Diagram showing the envelope of a wave packet

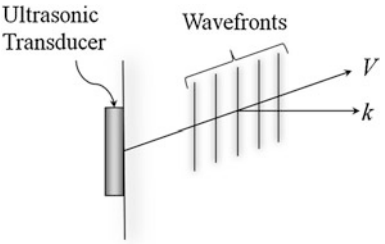

Fig. 2.3 Diagram showing plane waves propagating from an ultrasonic transducer in an anisotropic solid

In an anisotropic medium the physical difference between the phase and group velocity can be described by considering Fig. 2.3. The diagram shows a packet of plane waves propagating from an ultrasonic transducer. The wavefronts are parallel to the surface of the transducer and the velocities of the wavefronts propagate in the direction normal to the transducer surface given by the phase velocity. However, due to the anisotropy of material, the wave packet skews away from the normal direction and instead travels along the ray path. The velocity of the wave packet envelope is given by the group velocity.

Instead of the propagation of plane waves, the alternative case of a wave pulse propagating outwards from a point-source can also be considered. Figure 2.4 shows a plot of the wavefronts of the wave packet envelope propagating in an anisotropic solid from a point-source after a unit time. This plot is often referred to as the wavesurface and is equivalent to the plot of the group velocity as a function of ray path direction. In the propagation direction shown, the group velocity direction is clearly skewed from the wavenumber vector, which is always normal to the wavefront. Figure 2.4b shows how the group and phase velocities can be related through the skew angle ψ which can be expressed using the simple geometric equation:

$$c = V\cos(\psi) \tag{2.8}$$

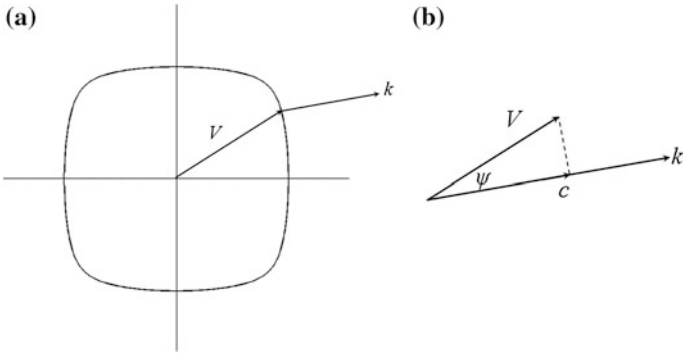

Fig. 2.4 **a** The quasi-longitudinal wavesurface of an anisotropic solid and **b** the geometric relationship between the group and phase velocities and the skew angle

2.2.3 Analytical Models

Analytical models to compute the phase and group velocities in an anisotropic material will now be derived. Tensor notation will be used for the derivation of these models for the compactness of this notation convention. In tensor notation, subscripts are used to show components of vectors in the three Cartesian coordinates, for example $x_i = \{x_1, x_2, x_3\}$. Einstein's summation convention is also used where variables with repeated subscripts are summed over all possible values of the subscripts (1, 2, 3) hence: $a_i b_i = \{a_1 b_1 + a_2 b_2 + a_3 b_3\}$. Differentiation with respect to direction is denoted using a comma, $u_{i,\,j} = \partial u_i / \partial x_j$, and therefore $u_{i,\,jk} = \partial^2 u_i / \partial x_j \partial x_k$. Differentiation with respect to time is indicated using a dot over the variable, $\dot{a} = \delta a / \delta t$.

2.2.3.1 Phase Velocity

The starting point to derive the equation for phase velocity in an anisotropic solid is Hooke's law. This law relates the stress σ acting on an elastic solid body to the strain ε. The stress at any point in a solid may be computed from the stresses acting on three mutually orthogonal faces. This can be described using the stress tensor. Tensors are often used to describe physical properties in a mathematical way so that the properties the tensor describes are invariant to a transformation in the coordinate system. The stress tensor, σ_{ij}, describes stress acting on the ith face in the jth direction of an elemental cube within the material. If the body is in equilibrium then the stress tensor must be symmetrical:

$$\sigma_{ij} = \sigma_{ji} \tag{2.9}$$

and hence the nine components of the tensor are made up of six independent elemental stresses. The elastic strain in a solid can also be described as a symmetrical tensor, ε_{ij}, and is related to the stress tensor through the elastic stiffness tensor C_{ijkl}:

$$\sigma_{ij} = C_{ijkl} \varepsilon_{kl} \tag{2.10}$$

The stiffness tensor is also symmetric:

$$C_{ijkl} = C_{jikl} = C_{ijlk} = C_{klij} \tag{2.11}$$

and hence the 81 (3^4) components can be reduced to 21 independent stiffness variables. The elastic constants of engineering materials are commonly expressed in Voigt notation as a symmetric 6×6 matrix:

Table 2.2 Indices contraction to swap between tensor and Voigt notation

Tensor indices	Voigt indices
$i = j = 1$	1
$i = j = 2$	2
$i = j = 3$	3
$i = 1, j = 2$ or $i = 2, j = 1$	6
$i = 1, j = 3$ or $i = 3, j = 1$	5
$i = 2, j = 3$ or $i = 3, j = 2$	4

$$C_{IJ} = \begin{bmatrix} C_{11} & C_{12} & C_{13} & C_{14} & C_{15} & C_{16} \\ - & C_{22} & C_{23} & C_{24} & C_{25} & C_{26} \\ - & - & C_{33} & C_{34} & C_{35} & C_{36} \\ - & - & - & C_{44} & C_{45} & C_{46} \\ - & - & - & - & C_{55} & C_{56} \\ - & - & - & - & - & C_{66} \end{bmatrix} \tag{2.12}$$

Therefore, the tensor notation must be contracted to the Voigt notation ($C_{ij,\ lk} \rightarrow C_{I,J}$) [18] and the appropriate indices swaps are shown in Table 2.2. Indice I in Voigt notation is calculated from tensor indices ij and likewise J from lk, so for example $C_{11,23}$ becomes $C_{1,4}$.

In the case of an isotropic material the elastic stiffness matrix in Voigt notation is:

$$C_{IJ} = \begin{bmatrix} C_{11} & C_{12} & C_{12} & 0 & 0 & 0 \\ - & C_{11} & C_{12} & 0 & 0 & 0 \\ - & - & C_{11} & 0 & 0 & 0 \\ - & - & - & C_{44} & 0 & 0 \\ - & - & - & - & C_{44} & 0 \\ - & - & - & - & - & C_{44} \end{bmatrix} \tag{2.13}$$

where:

$$C_{11} = \frac{E(1-\upsilon)}{(1+\upsilon)(1-2\upsilon)} \tag{2.14}$$

$$C_{12} = \frac{E\upsilon}{(1+\upsilon)(1-2\upsilon)} \tag{2.15}$$

$$C_{44} = \frac{1}{2}(C_{11} - C_{12}) = \frac{E}{2(1+\upsilon)} \tag{2.16}$$

The next step in computing the phase velocity is by using Newton's second law of motion to relate stress acting on a point in a solid to the motion of the particles in the solid. This law can be given in the form:

$$\rho \ddot{u}_i = \sigma_{ij,j} \tag{2.17}$$

where u_i is the displacement of a particle in the body in the ith direction. By differentiating Eq. (2.10) with respect to displacement, Newton's second law of motion and Hooke's law can be related through:

$$\rho \ddot{u}_i = C_{ijkl}\varepsilon_{kl,\,j} \tag{2.18}$$

The definition of elastic strain is:

$$\varepsilon_{kl} = \frac{1}{2}(u_{k,\,l} + u_{l,\,k}) \tag{2.19}$$

and hence Eq. (2.18) can be written as:

$$\rho \ddot{u}_i = \frac{1}{2} C_{ijkl}\left(u_{k,\,jl} + u_{l,\,jk}\right) \tag{2.20}$$

In tensor notation repeated indices may be swapped without changing the equation and therefore:

$$\rho \ddot{u}_i = C_{ijkl} u_{k,\,jl} \tag{2.21}$$

This is often referred to as Cauchy's law of motion. A solution to this equation can be assumed to take the form of a plane wave. This is useful because any wavefield can be described as a superposition of plane waves. The displacement of a particle at time t and distance x due to a one-dimensional plane wave can be described using:

$$u(x,t) = A cos(kx - \omega t) \tag{2.22}$$

where A is the wave amplitude. This is often expressed in exponential form using Euler's formula ($e^{ix} = cos(x) + i\ sin(x)$) as:

$$u(x,t) = Ae^{i(kx-\omega t)} \tag{2.23}$$

For a physical wave only the real part of this equation is used. A three-dimensional plane wave in tensor notation is therefore given by:

$$\ddot{u}_i = Ap_i e^{i(k_i x_i - \omega t)} \tag{2.24}$$

where p represents the polarization vector. To relate the plane wave solution to Eq. (2.21), the plane wave equation is first differentiated twice with respect to time:

$$\ddot{u}_i = -\omega^2 Ap_i e^{i(k_i x_i - \omega t)} \tag{2.25}$$

This is equivalent to:

$$\ddot{u}_i = -\omega^2 u_i \tag{2.26}$$

In a similar way, differentiating twice with respect to distance yields:

$$u_{k,jl} = -k_j k_l u_k \tag{2.27}$$

Therefore combining Eqs. (2.26) and (2.27) with Eq. (2.21) gives:

$$\rho\omega^2 u_i = C_{ijkl} k_j k_l u_k \tag{2.28}$$

The wave vector k_i is related to the wavenumber k through:

$$k_i = k n_i \tag{2.29}$$

where n_i represents the wavefront propagation direction. Therefore by substitution:

$$\rho\omega^2 u_i = C_{ijkl} k^2 n_j n_l u_k \tag{2.30}$$

Using the definition of phase velocity from Eq. (2.3) yields:

$$\rho c^2 u_i = C_{ijkl} n_j n_l u_k \tag{2.31}$$

This equation can be written in the form known as the Christoffel equation:

$$\left[\rho c^2 \delta_{ik} - C_{ijkl} n_j n_l\right][u_k] = 0 \tag{2.32}$$

where δ_{ik} is the Kronecker delta:

$$\delta_{ik} = \begin{cases} 1, \text{ if } i = k \\ 0, \text{ if } i \neq k \end{cases} \tag{2.33}$$

The Christoffel equation can be seen to be an eigenvalue equation. Therefore, with the appropriate material properties, this equation can then be solved using eigenvalue analysis to compute the phase velocities of all possible wave modes with a particular wavefront normal (i.e. phase velocity direction) specified by n_j. The solution to the Christoffel equation yields three eigenvalues related to the phase velocity of the three wave modes that can exist in an anisotropic solid. Each eigenvalue has a corresponding eigenvector describing the displacement caused by each mode. The polarization vector of the individual wave modes is given by:

$$p_i = \frac{u_i}{\sqrt{u_j u_j}} \tag{2.34}$$

When the polarization vector is parallel to the wavefront normal direction the wave is a pure longitudinal mode. The wave is pure shear when the polarization vector is perpendicular to the wavefront normal direction. If the polarization vector fulfils neither of these conditions, the wave propagates in a quasi-mode.

2.2.3.2 Group Velocity

One possible way to obtain the group velocity profile is via a graphical method [13]. In this method the reciprocal of the phase velocity is plotted in the direction of the wavenumber vector as shown in Fig. 2.5. The resulting plot is referred to as

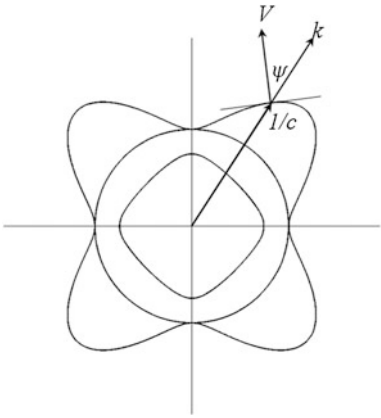

Fig. 2.5 Graphical method of computing the group velocity from the slowness surface

the slowness surface. The normal to the slowness surface is the direction of the group velocity. The angle between direction of the group velocity and the wavenumber vector yields the skew angle ψ. Hence, using Eq. (2.8) the group velocity can be computed.

However, practical implementation of this method is difficult due to numerical inaccuracies when measuring the normal to the slowness surface, especially as the slowness is a 3D surface. Therefore, an equation-based method is preferable. One approach to compute the group velocity is to consider the energy of a plane wave. These energy-based methods derive the energy velocity and then show how this is equal to the group velocity for lossless materials [10, 18]. The energy-based derivation is given in Appendix A. However, for the main body of this thesis, a simpler approach given by Merkulov [9] is used.

Starting from the definition of the group velocity in tensor form:

$$V_i = \frac{\partial \omega}{\partial k_i} \tag{2.35}$$

Now consider the Eq. (2.28) written using the polarization vector:

$$\rho \omega^2 p_i = C_{ijkl} k_k k_l p_j \tag{2.36}$$

Multiplying both sides by p_i yields:

$$\rho \omega^2 p_i p_i = C_{ijkl} k_k k_l p_j p_i \tag{2.37}$$

Because the polarization is a unit vector, ($p_i p_i = 1$), and therefore:

$$\rho \omega^2 = C_{ijkl} k_k k_l p_j p_i \tag{2.38}$$

Taking the derivative with respect to the wave vector, k_p, yields:

$$\rho \frac{\partial \omega^2}{\partial k_p} = C_{ijkl} p_j p_i \frac{\partial (k_k k_l)}{\partial k_p} \tag{2.39}$$

The right hand side of this equation can be solved using the product rule $(\partial(uv)/\partial x = u\partial v/\partial x + v\partial u/\partial x)$ and the left hand side using $\partial u/\partial n = \partial u/\partial c \times \partial c/\partial n$ where $u = c^2$. Therefore:

$$2\rho\omega\frac{\partial\omega}{\partial k_p} = C_{ijkl}p_j p_i\left(k_k\frac{\partial k_l}{\partial k_p} + k_l\frac{\partial k_k}{\partial k_p}\right) \tag{2.40}$$

$$2\rho\omega\frac{\partial\omega}{\partial k_p} = C_{ijkl}p_j p_i\left(k_k\delta_{lp} + k_l\delta_{kp}\right) \tag{2.41}$$

Using the properties of the Kronecker delta:

$$2\rho\omega\frac{\partial\omega}{\partial k_p} = C_{ijkp}p_j p_i k_k + C_{ijpl}p_j p_i k_l \tag{2.42}$$

Repeated indices can be swapped, and therefore:

$$2\rho\omega\frac{\partial\omega}{\partial k_p} = C_{ijkp}p_j p_i k_k + C_{ijpk}p_j p_i k_k \tag{2.43}$$

$$\rho\omega\frac{\partial\omega}{\partial k_j} = C_{ijkl}p_l p_i k_k \tag{2.44}$$

Rearranging and using the definition of the phase velocity yields:

$$\frac{\partial\omega}{\partial k_j} = \frac{k}{\rho\omega}C_{ijkl}p_l p_i n_k \tag{2.45}$$

$$\frac{\partial\omega}{\partial k_j} = \frac{C_{ijkl}n_k p_i p_l}{\rho c} \tag{2.46}$$

Finally, by referring to Eq. (2.35), it can be seen that:

$$V_j = \frac{C_{ijkl}n_k p_i p_l}{\rho c} \tag{2.47}$$

The group velocity is therefore the magnitude of the group velocity vector, V_j, which has its own propagation angle.

2.2.4 Results and Validation

The analytical models for waves propagating in a generic anisotropic material were applied to CMSX-4, the single crystal nickel-based superalloy considered throughout this thesis. The elastic properties of a cubic material such as CMSX-4 are given in Voigt notation as:

Table 2.3 Elastic constants and density of CMSX-4

Material property	Value at room temperature
C_{11}	235 GPa
C_{12}	142 GPa
C_{44}	131 GPa
ρ	8720 kg/m^3

$$C_{IJ} = \begin{bmatrix} C_{11} & C_{12} & C_{12} & 0 & 0 & 0 \\ C_{12} & C_{11} & C_{12} & 0 & 0 & 0 \\ C_{12} & C_{12} & C_{11} & 0 & 0 & 0 \\ 0 & 0 & 0 & C_{44} & 0 & 0 \\ 0 & 0 & 0 & 0 & C_{44} & 0 \\ 0 & 0 & 0 & 0 & 0 & C_{44} \end{bmatrix} \tag{2.48}$$

where $C_{44} \neq 0.5(C_{11}-C_{12})$. The elastic constants and density of CMSX-4 at room temperature are given in Table 2.3.

As Eq. (2.48) shows, the elastic properties of a cubic crystal can be described using just three independent variables, significantly less than the 21 variables needed to fully describe the most general anisotropic material. Therefore, in certain symmetry directions, simple relationships for the phase velocities can be achieved [21]. For example in the $< 001 >$ crystallographic directions in a cubic material the equations for the three wave modes are:

$$\rho c_{qL}^2 = C_{11} \tag{2.49}$$

$$\rho c_{qS_V}^2 = \rho c_{qS_H}^2 = C_{44} \tag{2.50}$$

where the subscript qL indicates the quasi-longitudinal modes, and qS_V and qS_H denote quasi-shear modes with vertical and horizontal polarization respectively. In the $< 011 >$ directions the phase velocities are:

$$\rho c_{qL}^2 = \frac{1}{2}(C_{11} + C_{12} + 2C_{44}) \tag{2.51}$$

$$\rho c_{qS_H}^2 = C_{44} \tag{2.52}$$

$$\rho c_{qS_V}^2 = \frac{1}{2}(C_{11} - C_{12}) \tag{2.53}$$

and finally in the $< 111 >$ directions:

$$\rho c_{qL}^2 = \frac{1}{3}(C_{11} + 2C_{12} + 4C_{44}) \tag{2.54}$$

$$\rho c_{qS_V}^2 = \rho c_{qS_H}^2 = \frac{1}{3}(C_{11} - C_{12} + C_{44}) \tag{2.55}$$

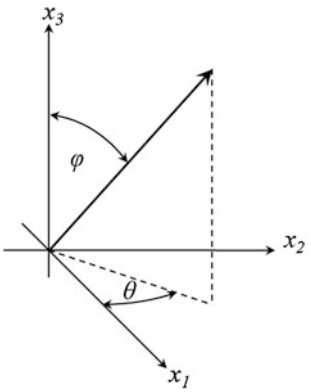

Fig. 2.6 Spherical Coordinates

The above equations can serve as useful checks to ensure computer implementations of the analytical velocity models are correct.

To compute the velocity profiles of the three wave modes in all directions in CMSX-4, a computer program was developed in MATLAB 7.5.0 (The MathWorks Inc., Massachusetts, USA). The propagation directions were defined using spherical coordinates:

$$n_i = \begin{bmatrix} \cos\theta \sin\varphi \\ \sin\theta \sin\varphi \\ \cos\varphi \end{bmatrix} \tag{2.56}$$

where θ is the azimuth angle and φ is the zenith angle, as shown in Fig. 2.6. The complete range of propagation directions were computed with θ varying from -180 to 180° and φ varying from 0 to 180°. First the phase velocity was computed using Eq. (2.32) and the eigenvalue subroutines available in MATLAB. To check that the code had been implemented correctly, the computed phase velocities were compared to the close form solutions given in Eqs. (2.49) to (2.55). The phase velocities and polarization vectors computed from the eigenvalues and eigenvectors of Eq. (2.32) respectively were then used in Eq. (2.47) for the group velocity vector, from which the magnitude and direction of the group velocity could be computed.

Figure 2.7 shows the computed wavesurfaces (a plot of the group velocity vector) of the three wave modes for the CMSX-4 crystal in the {001} crystallographic plane. The quasi-longitudinal mode is labelled qL. The quasi-shear wave mode with horizontal polarization is labelled qS_H. In the {001} plane the mode is a pure-shear mode with isotropic characteristics. This is not the case for the other crystallographic planes. The second quasi-shear mode is polarized in the vertical plane and is labelled qS_V. In this plane the qS_V wave mode shows a highly anisotropic wavesurface. The points labelled A and B on the wavesurface are a conical point and cusp respectively. Between these points a cone in the wavesurface occurs where the qS_V wave has three different group velocities. Figure 2.8, a plot of the slowness surface from CMSX-4 in the {001} plane, shows graphically

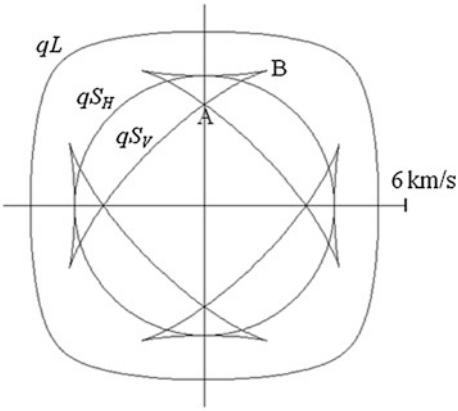

Fig. 2.7 The wavesurfaces of the three waves in single crystal CMSX-4. The plane shown is the {001} plane and the axes are aligned to the $< 001 >$ crystallographic directions. The points labelled A and B on the vertically polarised quasi-shear wave shows a conical point and a cusp respectively

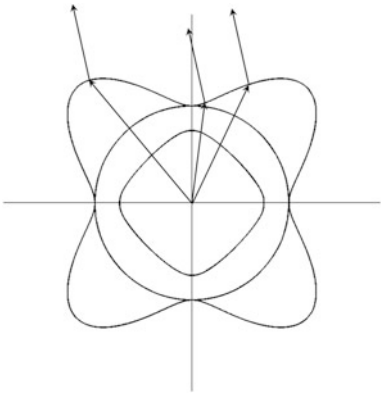

Fig. 2.8 A schematic diagram of the slowness surface of CMSX-4, showing how three separate wavefront directions can produce three different group velocities in a single group velocity direction

how three different phase vectors can produce three group velocity vectors in the same ray direction but with different magnitudes.

Figure 2.9 shows the quasi-longitudinal group velocity profile computed at all angles. This mode is shown in more detail as this is the mode that will be used later in the ultrasonic array imaging. The profile is shown as a spherical plot where the gray-scale represents the different velocities. The model predicts that the velocity varies from a minimum of 5.194 km/s in the $< 001 >$ crystallographic directions to a maximum of 6.316 km/s in the $< 111 >$ directions. The velocity profile can be seen to have reflective symmetry about the {001} planes.

2.3 Wave Amplitude from a Point-force on an Infinite Half-Space

Any arbitrary transducer can be modelled by the superposition of point-forces on the surface of the transducer. To be clear, a point-force refers to a force acting on a point in a single direction. These models can be used to compute the ultrasonic

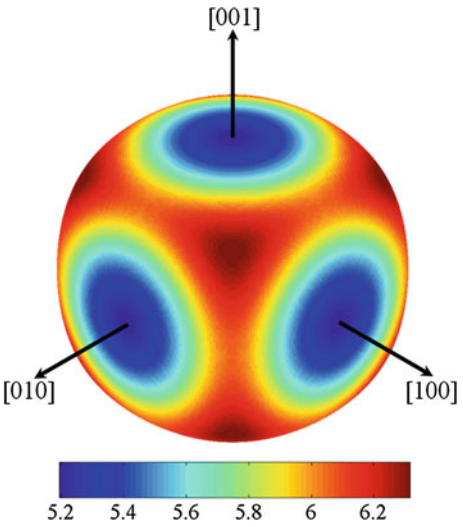

Fig. 2.9 A colourmap showing the qL group velocity profile in CMSX-4. Velocities are shown in units of km/s

field created by the transducer. This in turn enables the prediction of the amplitude response from a given reflector at different locations relative to the insonifying transducer in an anisotropic solid. These concepts will be discussed further in the next chapter. The model to compute the amplitude of a wave propagating from a point-force acting on the surface of an infinite anisotropic half-space in different directions will now be presented.

2.3.1 Analytical Model

The analytical model comprises two parts. The first uses the reciprocity theorem and reflection coefficients to compute the amplitude of waves propagating from a point-force acting on an anisotropic half-space due to Wu et al. [15]. The second part uses the anisotropic Green's function given by Buchwald [11], which describes the amplitude of a wave from a point-force in an infinite anisotropic as this is required as an input to the reciprocity calculations.

However, before the analytical models are presented it is often useful to rotate the elastic stiffness matrix to account for a rotation of the single crystal, or indeed any anisotropic material, relative to the surface on which the point-force is applied. This can be achieved using Bond matrix multiplication:

$$\left[C'_{IJ}\right] = [M][C_{IJ}][M^T] \tag{2.57}$$

where C'_{IJ} is the transformed elastic stiffness matrix, the superscript T indicates the transpose, and M is the Bond matrix given by:

$$[M] = [M_1][M_2][M_3] \tag{2.58}$$

The components of the Bond matrix can be given by three consecutive rotations θ_1, θ_2 and θ_3 about the three local Cartesian axes:

$$[M_1] = \begin{bmatrix} cos(\theta_1)^2 & sin(\theta_1)^2 & 0 & 0 & 0 & sin(2\theta_1) \\ sin(\theta_1)^2 & cos(\theta_1)^2 & 0 & 0 & 0 & -sin(2\theta_1) \\ 0 & 0 & 1 & 0 & 0 & 0 \\ 0 & 0 & 0 & cos(\theta_1) & -sin(\theta_1) & 0 \\ 0 & 0 & 0 & sin(\theta_1) & cos(\theta_1) & 0 \\ -1/2sin(2\theta_1) & 1/2sin(2\theta_1) & 0 & 0 & 0 & cos(2\theta_1) \end{bmatrix} \tag{2.59}$$

$$[M_2] = \begin{bmatrix} \cos(\theta_2)^2 & 0 & \sin(\theta_2)^2 & 0 & -\sin(2\theta_2) & 0 \\ 0 & 1 & 0 & 0 & 0 & 0 \\ \sin(\theta_2)^2 & 0 & \cos(\theta_2)^2 & 0 & \sin(2\theta_2) & 0 \\ 0 & 0 & 0 & \cos(\theta_2) & 0 & \sin(\theta_2) \\ 1/2\sin(2\theta_2) & 0 & -1/2\sin(2\theta_2) & 0 & \cos(2\theta_2) & 0 \\ 0 & 0 & 0 & -\sin(\theta_2) & 0 & \cos(\theta_2) \end{bmatrix} \tag{2.60}$$

$$[M_3] = \begin{bmatrix} 1 & 0 & 0 & 0 & 0 & 0 \\ 0 & cos(\theta_3)^2 & sin(\theta_3)^2 & sin(2\theta_3) & 0 & 0 \\ 0 & sin(\theta_3)^2 & cos(\theta_3)^2 & -sin(2\theta_3) & 0 & 0 \\ 0 & -1/2sin(2\theta_3) & 1/2sin(2\theta_3) & cos(2\theta_3) & 0 & 0 \\ 0 & 0 & 0 & 0 & cos(\theta_3) & sin(\theta_3) \\ 0 & 0 & 0 & 0 & -sin(\theta_3) & cos(\theta_3) \end{bmatrix} \tag{2.61}$$

Other rotation conventions can be successfully used, although appropriate changes to the Bond matrices would be required.

2.3.1.1 Normal Point-force on an Anisotropic Half-Space

The first step in the analytical model is to compute the wave vectors of the three possible reflected wave modes (one quasi-longitudinal and two quasi-shear) caused by an incident wave reflecting off a solid-void interface. From Snell's law, the projections of all the wave vectors on the interface surface must be equal and in the same plane as the incident wave (see Chap. 8 in Fedorov [10] or [22, 23]). In other words, the s_1 component of the slowness vector, s_i, is equivalent for all modes, as shown schematically in Fig. 2.10. In this example the incident and reflected waves are in the s_1–s_3 plane and therefore they have no s_2 component. Hence the remaining component of the slowness vector, s_3, can be found graphically by

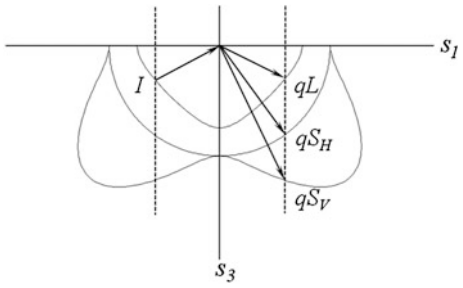

Fig. 2.10 Diagram showing the slowness surfaces of the three reflected wave modes from an incident wave

plotting the slowness surfaces of the three wave modes, and finding where the surfaces are intercepted by a line drawn at s_1.

To find the s_3 vector mathematically, the Christoffel equation is written in terms of the slowness vector:

$$\left|C_{ijkl}s_j s_k - \rho\delta_{il}\right| = 0 \tag{2.62}$$

By defining G_{il} as:

$$|G_{il}| = \left|C_{ijkl}s_j s_k - \rho\delta_{il}\right| \tag{2.63}$$

the terms can be expanded to give:

$$\begin{aligned} G_{11} &= C_{11}s_1^2 + C_{16}s_1s_2 + C_{15}s_1s_3 + C_{61}s_2s_1 + C_{66}s_2^2 + C_{65}s_2s_3 + C_{51}s_3s_1 \\ &\quad + C_{56}s_3s_2 + C_{55}s_3^2 - \rho \end{aligned} \tag{2.64}$$

$$\begin{aligned} G_{12} &= G_{21} \\ &= C_{16}s_1^2 + C_{12}s_1s_2 + C_{14}s_1s_3 + C_{66}s_2s_1 + C_{62}s_2^2 + C_{64}s_2s_3 + C_{56}s_3s_1 \\ &\quad + C_{52}s_3s_2 + C_{54}s_3^2 \end{aligned} \tag{2.65}$$

$$\begin{aligned} G_{13} &= G_{31} \\ &= C_{15}s_1^2 + C_{14}s_1s_2 + C_{13}s_1s_3 + C_{65}s_2s_1 + C_{64}s_2^2 + C_{63}s_2s_3 + C_{55}s_3s_1 \\ &\quad + C_{54}s_3s_2 + C_{53}s_3^2 \end{aligned} \tag{2.66}$$

$$\begin{aligned} G_{22} &= C_{66}s_1^2 + C_{62}s_1s_2 + C_{64}s_1s_3 + C_{26}s_2s_1 + C_{22}s_2^2 + C_{24}s_2s_3 + C_{46}s_3s_1 \\ &\quad + C_{42}s_3s_2 + C_{44}s_3^2 - \rho \end{aligned} \tag{2.67}$$

$$\begin{aligned} G_{23} &= G_{32} \\ &= C_{65}s_1^2 + C_{64}s_1s_2 + C_{63}s_1s_3 + C_{25}s_2s_1 + C_{24}s_2^2 + C_{23}s_2s_3 + C_{45}s_3s_1 \\ &\quad + C_{44}s_3s_2 + C_{43}s_3^2 \end{aligned} \tag{2.68}$$

$$\begin{aligned} G_{33} &= C_{55}s_1^2 + C_{54}s_1s_2 + C_{53}s_1s_3 + C_{45}s_2s_1 + C_{44}s_2^2 + C_{43}s_2s_3 + C_{35}s_3s_1 \\ &\quad + C_{34}s_3s_2 + C_{33}s_3^2 - \rho \end{aligned} \tag{2.69}$$

Slowness vector component s_2 is set to zero to yield:

$$G_{11} = C_{11}s_1^2 + 2C_{15}s_1s_3 + C_{55}s_3^2 - \rho \tag{2.70}$$

$$G_{12} = C_{16}s_1^2 + (C_{14} + C_{56})s_1s_3 + C_{54}s_3^2 \tag{2.71}$$

$$G_{13} = C_{15}s_1^2 + (C_{13} + C_{55})s_1s_3 + C_{53}s_3^2 \tag{2.72}$$

$$G_{22} = C_{66}s_1^2 + 2C_{64}s_1s_3 + C_{44}s_3^2 - \rho \tag{2.73}$$

$$G_{23} = C_{65}s_1^2 + (C_{63} + C_{45})s_1s_3 + C_{43}s_3^2 \tag{2.74}$$

$$G_{33} = C_{55}s_1^2 + 2C_{53}s_1s_3 + C_{33}s_3^2 - \rho \tag{2.75}$$

Therefore, any given s_1 yields a sextic equation which can be solved for s_3. This sextic equation will give six slowness vectors for any s_1 input. However, the solutions that are valid are ones that cause the energy to be reflected back into the solid and inappropriate solutions are discarded.

Having computed the slowness vector of each reflected wave mode, the polarization, p_i, of the three waves must also be found. This is achieved by inserting the slowness vector values into the modified Christoffel Eq. (2.62) and computing the eigenvectors to give the wave polarizations.

Next, the amplitudes of the reflected waves can be found by considering the stresses at the interface. The stress caused by a propagating wave can be expressed as:

$$\sigma_{ij} = C_{ijkl}\varepsilon_{kl} = C_{ijkl}\frac{du_k}{dx_l} \tag{2.76}$$

Again, assuming the solution takes the form of a plane wave and differentiating the equation of the plane wave (2.24) with respect to direction yields:

$$\sigma_{ij} = C_{ijkl}Ap_lk_lu_k \tag{2.77}$$

The stresses of the incident wave and the three reflected waves that have a component normal to the interface must balance. These are σ_{33}, σ_{13} and σ_{23} and hence:

$$\sigma_{33}^I = \sigma_{33}^{qL} + \sigma_{33}^{qS_H} + \sigma_{33}^{qS_V} \tag{2.78}$$

$$\sigma_{13}^I = \sigma_{13}^{qL} + \sigma_{13}^{qS_H} + \sigma_{13}^{qS_V} \tag{2.79}$$

$$\sigma_{23}^I = \sigma_{23}^{qL} + \sigma_{23}^{qS_H} + \sigma_{23}^{qS_V} \tag{2.80}$$

Here the superscripts I, qL, qS_V, qS_H refer to the incident wave, the reflected quasi-longitudinal wave and the reflected quasi-shear waves with vertical and horizontal polarization respectively. There must also be continuity of the displacement vectors at the surface of the half-space. Therefore combining Eq. (2.77) with Eqs. (2.78) to (2.80) and removing the constant variables gives:

$$C_{33kl}A^I p_l^I k_k^I = C_{33kl}A^{qL} p_l^{qL} k_k^{qL} + C_{33kl}A^{qS_H} p_l^{qS_H} k_k^{qS_H} + C_{33kl}A^{qS_V} p_l^{qS_V} k_k^{qS_V} \quad (2.81)$$

$$C_{13kl}A^I p_l^I k_k^I = C_{13kl}A^{qL} p_l^{qL} k_k^{qL} + C_{13kl}A^{qS_H} p_l^{qS_H} k_k^{qS_H} + C_{13kl}A^{qS_V} p_l^{qS_V} k_k^{qS_V} \quad (2.82)$$

$$C_{23kl}A^I p_l^I k_k^I = C_{23kl}A^{qL} p_l^{qL} k_k^{qL} + C_{23kl}A^{qS_H} p_l^{qS_H} k_k^{qS_H} + C_{23kl}A^{qS_V} p_l^{qS_V} k_k^{qS_V} \quad (2.83)$$

Grouping terms of unknown amplitudes gives the following:

$$\begin{pmatrix} C_{33kl}A^I p_l^I k_k^I \\ C_{13kl}A^I p_l^I k_k^I \\ C_{23kl}A^I p_l^I k_k^I \end{pmatrix} = \begin{pmatrix} C_{33kl}p_l^{qL} k_k^{qL} & C_{33kl}p_l^{qS_H} k_k^{qS_H} & C_{33kl}p_l^{qS_V} k_k^{qS_V} \\ C_{13kl}p_l^{qL} k_k^{qL} & C_{13kl}p_l^{qS_H} k_k^{qS_H} & C_{13kl}p_l^{qS_V} k_k^{qS_V} \\ C_{23kl}p_l^{qL} k_k^{qL} & C_{23kl}p_l^{qS_H} k_k^{qS_H} & C_{23kl}p_l^{qS_V} k_k^{qS_V} \end{pmatrix} \begin{pmatrix} A^{qL} \\ A^{qS_H} \\ A^{qS_V} \end{pmatrix} \quad (2.84)$$

Therefore, for a given incident wave the amplitudes of the reflected waves can be computed. These amplitudes can be used along with the reciprocity theorem to compute the wave amplitude from a point-force. The reciprocity theorem used in this case can be explained by considering Fig. 2.11. An incident plane wave can be produced by a force F acting on a remote point in the solid, labelled R, in the direction of the polarization vector of the incident plane wave. This force causes a normal particle displacement on the free surface. The amplitude of this normal displacement on the free surface is given by the superposition of the incident and reflected waves:

$$u_N = A^I p_N^I + A^{qL} p_N^{qL} + A^{qS_V V} p_N^{qS_V} + A^{qS_H} p_N^{qS_H} \quad (2.85)$$

where the subscript N indicates the normal direction. From the reciprocity theorem, a normal force acting on the free surface will cause a particle displacement at R with a magnitude described by the same equation. Therefore all that is required now is a relationship between the force in the solid and the amplitude of the incident wave. This can be computed using the anisotropic Green's function.

2.3.1.2 Green's Function for Anisotropic Media

In an infinite solid the point-force solution to the wave equation is referred to as the Green's function. The displacement u_i at a distance x and time t due to a point-

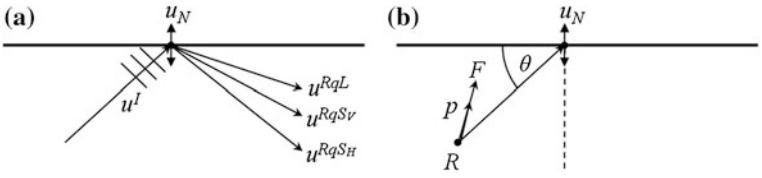

Fig. 2.11 Diagram showing reciprocity theorem that is used to calculate the directivity pattern

force at x_0 and t_0 orientated in the nth Cartesian axis is given by the Green's function G:

$$u_i(x,t) = G_{in}(x,\ t;\ x_0 t_0) \tag{2.86}$$

The time dependence of the force is assumed to be given by a spike, or delta, function. To compute the Green's function for an anisotropic solid, the derivation given by Buchwald [11] using the asymptotic method due to Lighthill [12] is used. This derivation is repeated briefly by Vavryčuk [24] and in detail in Sect. 2.5.5 of Červený [18].

The starting point for the derivation is to return to Cauchy's equation of motion given by Eq. (2.21) but now to include a body force term F:

$$\rho \ddot{u}_i = C_{ijkl} u_{k,\,jl} + \rho F_i \tag{2.87}$$

The body force is assumed to take a general source function representing a small harmonic source given by:

$$F_i = e^{-i\omega t} \iiint_{-\infty}^{\infty} \overline{F}_i e^{ik_j x_j} dk_1 dk_2 dk_3 \tag{2.88}$$

When this force is replaced by a delta function later, the Green's function will be obtained. Making use of the Fourier transform:

$$\overline{y}(k) = \int_{\mathbb{R}^n} y(x) e^{-ikx} dx \tag{2.89}$$

$$y(x) = \frac{1}{(2\pi)^n} \int_{\mathbb{R}^n} \overline{y}(k) e^{ikx} dk \tag{2.90}$$

the 3-D Fourier transform $\overline{F}$ is:

$$\overline{F_i} = \frac{1}{8\pi^3} e^{-i\omega t} \iiint_{-\infty}^{\infty} F_i e^{-ik_j x_j} dx_1 dx_2 dx_3 \tag{2.91}$$

Displacement can also be expressed as:

$$u_i = e^{-i\omega t} \iiint_{-\infty}^{\infty} \overline{u_i} e^{ik_j x_j} dk_1 dk_2 dk_3 \tag{2.92}$$

$$\overline{u_i} = \frac{1}{8\pi^3} e^{-i\omega t} \iiint_{-\infty}^{\infty} u_i e^{-ik_j x_j} dx_1 dx_2 dx_3 \tag{2.93}$$

Therefore, the appropriate differentiation of the above equation and substitution of the results along with Eq. (2.88) into Eq. (2.87) yields:

$$\rho\omega^2\overline{u}_i = C_{ijkl}k_jk_l\overline{u}_k + \rho\overline{F}_i \tag{2.94}$$

This is a set of three linear equations, the solution to which is given by the inversion:

$$\overline{u}_i = \frac{B_{ki}\overline{F}_i}{\rho\det(\Gamma_{ik})} \tag{2.95}$$

where det denotes the determinant of the matrix, and:

$$\Gamma_{ik} = C_{ijkl}k_jk_l - \rho\omega^2\delta_{ik} \tag{2.96}$$

B_{ik} are the cofactors of Γ_{ik}. Therefore inserting (2.95) into Eq. (2.92) yields:

$$u_i = e^{-i\omega t}\int_{-\infty}^{\infty}\int\int\frac{B_{ki}\overline{F}_i}{\rho\det(\Gamma_{ik})}e^{ik_jx_j}dk_1dk_2dk_3 \tag{2.97}$$

To arrive at Green's function the general force term is replaced by a spike force at x_0 which is orientated along the x_n axis applied at time t_0:

$$F_i = \delta_{in}\Delta(t-t_0)\Delta(x-x_0) \tag{2.98}$$

where δ_{in} is the Kronecker delta function and Δ is the Dirac delta function [18]. By referring to Eq. (2.91) the following expression is obtained for the spike force in the frequency/wavenumber domain:

$$\overline{F}_i = \frac{1}{8\pi^3}\delta_{in}e^{-ik_0x_0} \tag{2.99}$$

Therefore, using $k_i = \omega s_i$, where s_i is the slowness vector (the reciprocal of the phase velocity) yields:

$$G_{in} = \frac{e^{-i\omega t}}{8\pi^3}\int_{-\infty}^{\infty}\int\int\frac{B_{ki}\delta_{in}}{\rho\det(\Gamma_{ik})}e^{i(k_jx_j-k_0x_0)}dk_1dk_2dk_3 \tag{2.100}$$

Therefore, the Green's function can be computed from the 3D inverse Fourier transform given above. This can be thought of as a superposition of plane waves at arbitrary propagation directions with arbitrary phase velocity. The above equation can be simplified using some involved mathematics. First the residual theorem, (for example see Sect. 1.9 of [4]) is implemented to reduce the volume integral into a surface integral, which physically represents a superposition of plane waves at arbitrary angles but with a phase velocity given by the Christoffel equation. The Green's function can then be computed asymptotically, meaning that the function is computed in the far-field a long distance away from the source, using the method

of stationary phase (see Sect. 7.5 of [4]). Therefore, it can be shown that the asymptotic Green's function in an anisotropic material at distance d is given by [18]:

$$G(d)_{in} \approx \frac{p_i p_n}{4\pi\rho\sqrt{|K|Vd}} e^{i\left(kd-\omega t+\frac{\pi}{2}\sigma_0\right)} \tag{2.101}$$

where:

$$\sigma_0 = 1 - \frac{1}{2}sgn(\kappa_1) - \frac{1}{2}sgn(\kappa_2) \tag{2.102}$$

κ_1 and κ_2 are the principle curvatures of the slowness surface and sgn denotes the sign. $K = \kappa_1\kappa_2$ and is referred to as the Gaussian curvature. A method to compute the Gaussian curvature is given in Appendix C. The quantities that vary with direction in the above equation: group velocity, wave vector, and curvature, must be evaluated in the direction of interest.

The anisotropic Green's function shows that the amplitude response from a point-force decreases linearly with distance from the source and is proportional to the reciprocal of the square root of the slowness surface curvature. As this expression contains the reciprocal of the slowness surface curvature, this expression cannot be applied to surfaces with zero curvature, such as the cuspidal edges shown at point B in Fig. 2.7. However, for the qL wavesurface in CMSX-4, the equation is valid at all points.

Therefore, by using Eq. (2.101), the wave amplitude due to a force in an anisotropic solid can be computed. This wave amplitude can be inserted into Eq. (2.84) to find the wave amplitude of the reflected waves. The incident and reflected wave amplitudes are finally used in Eq. (2.85) to compute the wave amplitude due to a normal point-force on the surface of an anisotropic half-space.

2.3.2 Results and Validation

The analytical model was implemented in MATLAB and applied to CMSX-4. The analytical model was used to compute the qL wave mode, as this is the only wave mode that will be used for imaging in subsequent chapters. The computational scheme was as follows. Initially, the elastic tensor was transformed using the Bond matrices to align the crystal axes with the axes of the model using Eq. (2.57). Incident qL plane waves were simulated for angles $-90°$ to $+90°$ relative to the normal to the surface, in $1°$ increments. At each direction the slowness vector describing the incident plane wave was split into its s_1 and s_3 components. The slowness vectors were found for the three reflected wave modes by solving Eq. (2.63) and selecting the results that corresponds to the back reflected waves. The polarization vector of each reflected wave mode was found using (2.62). The slowness and polarization vectors were then used to compute the reflection

coefficients using (2.84) which gave the beam directivity due to the free surface in Eq. (2.85). This equation was then multiplied by the anisotropic Green's function, Eq. (2.101), to compute the amplitude of the initial incident plane wave to then compute the final wave amplitude at each direction due to a normal point-force on the CMSX-4 surface. The amplitude was stored as a function of ray direction rather than wavefront normal directions.

As a first check, the model described above was used to compute the beam amplitudes of the longitudinal wave mode from a normal point-force acting on the surface of a isotropic half-space and this was compared to close-form solutions as detailed in Appendix B. The two models were found to be numerically equal to six significant figures.

A numerical finite element (FE) model was developed to validate the analytical model. FE analysis works by dividing a complex model into small, simple elements formed from interconnected nodes. The true displacement field within the elements is approximated by simple functions, referred to as shape functions. Equations are derived to relate the element node forces and displacement based on these shape functions. The equations of the individual elements are assembled in global matrices that describe the behaviour of the entire model. For the FE models described in this thesis, explicit time-marching methods were used to simulate the displacements in the mesh due to a dynamic loading by computing the response at small time-increments. Provided the model elements are sufficiently small, as is the time step over which the calculations are performed, the model will be highly accurate and contain all the wave modes that can be generated. However, due to the number of elements required to obtain a result with sufficient accuracy, FE models demand high computer memory and tend to be much slower than the equivalent analytical solutions. The accuracy of FE models for computing beam amplitude in isotropic media is discussed in Appendix B.

The FE model was developed in the commercial FE modelling software package ABAQUS 6.6 (SIMULIA, Providence RI, USA). The model is shown schematically in Fig. 2.12. The model consisted of three-dimensional cuboid elements formed from eight nodes making up a grid that was 4 nominal wavelengths long by 4 wavelengths deep and 1 wavelength thick, using 100 elements per wavelength. Here the nominal wavelength refers to the wavelength of the slowest qL group velocity as predicted by the analytical model. To reduce the model size, symmetric boundary conditions were used about the x – z and y – z planes at the origin. This was achieved by forcing the displacements in the x direction to zero for nodes that were located at $x = 0$. Likewise y displacements for nodes at $y = 0$ were forced to zero. A point-force was applied to a single node in the model to produce a one cycle pulse of 10 MHz centre frequency. Monitoring nodes were selected that were nominally at 3 wavelengths from the point-force at an angle of 0 to 90° in 1° increments. Due to the discretisation of the FE mesh the nodes were not generally at these nominal positions and so the actual distances and angles were computed and stored. The monitoring nodes had to be placed sufficiently far from the point-force to ensure the three wave modes were time-resolved and could therefore be separated. The Cartesian coordinate axes of the FE model

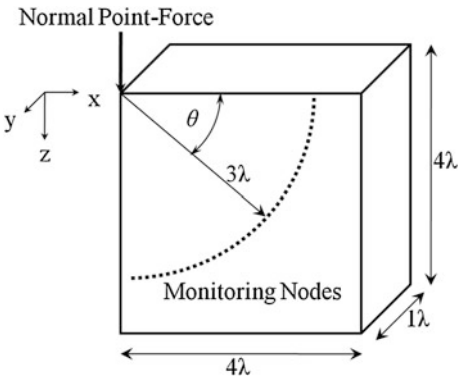

Fig. 2.12 Schematic diagram showing the finite element wave amplitude model

were aligned with the $< 001 >$ crystallographic directions and the monitoring nodes were placed in the {001} plane. The model was run in the time-domain using a time step of 0.5 ns.

Figure 2.13 shows the results of these models computed for a point-force acting normal to the surface with monitoring nodes in the {001} plane at an angle of 0 to 180° in incremental step of 1° with the *x, y* and *z* model axes aligned with the $< 001 >$ crystallographic directions. Figure 2.13c shows the absolute wave amplitude from the normal point-force whereas Fig. 2.13a and b show the components of the wave amplitude in the transverse directions (*x*) and the normal direction (*z*) respectively. The amplitudes have been normalised to the maximum amplitude value. The two models predict that the amplitude in the remaining direction, that is the normal to the {001} plane (*y*), is zero. Both models show excellent agreement apart from a small discrepancy around 90° with a maximum error of 10 %. It is thought that the error comes from the fact that the Green's function used in the analytical model is asymptotic. Therefore, it is only exact at very large distances between the source and receiver, whereas, the FE model used a distance of 3 wavelengths to compute the beam amplitude. The models show that the maximum ultrasonic energy in the {001} plane is in the $< 011 >$ direction, which is the direction that has the largest group velocity in this plane. The main discrepancy between the two models is in the direction along the surface where the analytical model predicts zero wave amplitude but the FE model result is non-zero. This is due to the surface waves in the FE model which are not accounted for in the analytical model.

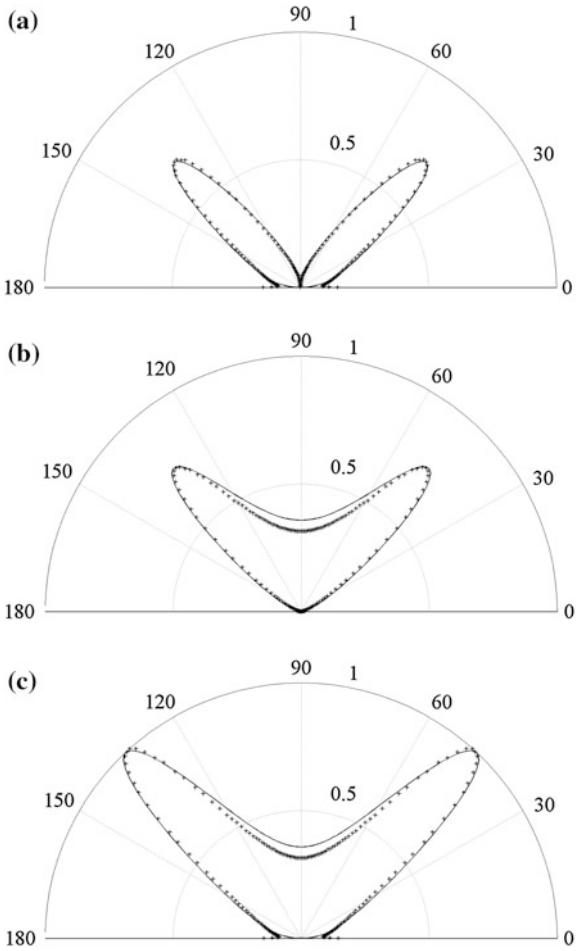

Fig. 2.13 Polar plots showing the beam directivity in the {001} plane with the graphs axes aligned with the $< 001 >$ crystallographic direction from a normal point-force. The plots shows the amplitude in (**a**) the x-direction, (**b**) the z-direction, and (**c**) as an absolute value found using the analytical model (*solid line*) and the FE model (crosses). The amplitudes have been normalised to the maximum amplitude value in this plane

2.4 Summary

This chapter has provided an introduction to the propagation of bulk waves in anisotropic solids. Analytical models have been developed to compute the velocity profiles and wave amplitudes of the three bulk wave modes in anisotropic solids. The models have been applied to CMSX-4 (a single crystal nickel-based super-alloy) and the models have been validated using results from numerical finite element models. The analytical models developed will be used in the next chapter. to correct ultrasonic imaging algorithms to account for wave propagation in anisotropic solids

References

1. Love AEH (1944) A treatise on the mathematical theory of elasticity, 4th edn. Dover Publications, New York
2. Green G (1839) On the propagation of light in crystallized media. Trans Cambridge Philos Soc 7(2):121–140
3. Christoffel EB (1877) Ueber die Fortpflanzung von Stössen durch elastische fest Körper. Annali di Matematic 8:193–243
4. Achenbach JD (1975) Wave propagation in elastic solids. Elsevier Science Publishers B. V, Amsterdam
5. Musgrave MJP (1970) Crystal acoustics. Holden-Day, London
6. Kelvin L (1904) Baltimore lectures on molecular dynamics and the wave theory of light. C. J. Clay and Sons, London
7. Musgrave MJP (1954) On the propagation of elastic waves in aeolotropic media. I. general principles. Proc R Soc A 226:339–355
8. Synge JL (1956) Elastic waves in anisotropic media. J Math Phys 35:323–334
9. Merkulov LG (1963) Ultrasonic waves in crystals. Appl Mater Res 2:231–240
10. Fedorov FI (1968) Theory of elastic waves in crystals. Plenum Press, New York
11. Buchwald VT (1959) Elastic waves in anisotropic media. In: Proceedings of the royal society of London. series A, Mathematical and physical sciences. pp 563–580
12. Lighthill MJ (1960) Studies on Magneto-Hydrodynamic waves and other anisotropic wave motions. Philos Trans R Soc A 252:397–430
13. Burridge R (1971) Lamb's problem for an anisotropic half-space. Q J Mech Appl Math 24:81–98
14. Mourad A, Deschamps M (1995) Lamb's problem for an anisotropic half-space studied by the Cagniard de Hoop method. J Acoust Soc Am 97(5):3194–3197
15. Wu K, Nagy PB, Adler L (1990) Far field radiation of a point source on the free surface of semi-infinite anisotropic solids. Rev Prog Quant Nondestr Eval 9:149–156
16. Wu K, Nagy PB, Adler L (1991) Far-field radiation of a vibrating point source in anisotropic media. J Nondestr Eval 10(2):71–78
17. Auld BA (1973) Acoustic fields and waves in solids. Vol 1 and 2, Wiley, New York
18. Červený V (2001) Seismic ray theory. Cambridge University Press, Cambridge
19. Farnell GW (1978) Types and properties of surface waves. In: Oliner AA (ed) Topics in applied physics, Springer-Verlag, Berlin, p 13–59
20. Rose JL (1999) Ultrasonic waves in solid media. Cambridge University Press, Cambridge
21. Miller GF, Musgrave MJP (1956) On the propagation of elastic waves in aeolotropic media. III. Media of cubic symmetry. Proc R Soc A 236:352–383
22. Henneke EG (1972) Reflection-refraction of a stress wave at a plane boundary between anisotropic media. J Acoust Soc Am 51(1):210–217
23. Rokhlin SI, Bolland TK, Adler L (1986) Reflection and refraction of elastic waves on a plane interface between two generally anisotropic media. J Acoust Soc Am 74(4):906–918
24. Vavrycuk V (2007) Asymptotic Green's function in homogeneous anisotropic viscoelastic media. Proc R Soc A 463:2689–2707

http://www.springer.com/978-3-319-02516-2

The Development of a 2D Ultrasonic Array Inspection for Single Crystal Turbine Blades

Lane, C.

2014, IX, 133 p. 80 illus., 12 illus. in color., Hardcover
ISBN: 978-3-319-02516-2